

Tracing very high energy neutrinos from cosmological distances in ice

J. Jones¹, I. Mocioiu^{1,3}, M. H. Reno² and I. Sarcevic^{1,3}

¹ Department of Physics, University of Arizona, Tucson, Arizona 85721, USA

² Department of Physics and Astronomy, University of Iowa, Iowa City, Iowa 52242 USA

³ KITP, UCSB, Santa Barbara, CA 93106

Abstract

Astrophysical sources of ultrahigh energy neutrinos yield tau neutrino fluxes due to neutrino oscillations. We study in detail the contribution of tau neutrinos with energies above 10^6 GeV relative to the contribution of the other flavors. We consider several different initial neutrino fluxes and include tau neutrino regeneration in transit through the Earth and energy loss of charged leptons. We discuss signals of tau neutrinos in detectors such as IceCube, RICE and ANITA.

1 Introduction

Very high energy neutrinos can be unique probes of both astrophysics and particle physics. They point back to their sources, escape from the most extreme environments and have energies much higher than those available in colliders.

The SuperKamiokande experimental data on atmospheric neutrinos [1] shows evidence of nearly maximal $\nu_\mu \leftrightarrow \nu_\tau$ mixing. As a result, astrophysical sources of ν_μ become sources of ν_μ and ν_τ in equal proportions after oscillations over astronomical distances [2]. We do not differentiate between neutrinos and antineutrinos, since they can not be distinguished experimentally. The neutral current cross sections for ν_μ and ν_τ are identical, and above ~ 1 TeV the charged current cross sections are identical as well. Nevertheless, signals from ν_τ have the potential to contribute differently from ν_μ 's because their propagation through matter is different. Tau neutrinos produce tau leptons via charged current interactions in the Earth. Having a short lifetime, the tau leptons decay producing ν_τ which then interact and produce τ , resulting in a cascade that produces ν_τ and τ with energies lower than the original flux [3, 4]. The leptonic tau decays also produce secondary ν_μ and ν_e neutrinos [23]. All neutrinos from this cascade can then interact in the detector. The decays of taus in the detector also contribute to the signal [5, 6]. For muons, the electromagnetic energy loss coupled with the long muon lifetime make regeneration of ν_μ from muon decay negligible and high energy ν_μ 's get large attenuation as they propagate through the Earth.

Signals of neutrino interactions in the rock below the ice or in ice depend on the energy and flavor of the neutrino. Muon neutrino charged current (CC) conversions to muons are noted by the Cherenkov signal of upward going muons in a detector such as IceCube [7]. High energy electromagnetic showers from $\nu_e \rightarrow e$ CC interactions produce Cherenkov radiation which is coherent for radio wavelengths [8]. The Radio Ice Cherenkov Experiment (RICE) has put limits on incident isotropic electron neutrino fluxes which produce downward-going electromagnetic showers [9]. The Antarctic Impulsive Transient Antenna (ANITA) also uses the ice as a neutrino converter [10]. These balloon missions will monitor the ice sheet for refracted radio frequency signals with an effective telescope area of 1M km². All flavors of neutrinos produce hadronic showers. In addition, tau decays contribute to both electromagnetic and hadronic showers that could be detected by IceCube, RICE or ANITA.

In this paper, we investigate the effect of ν_τ regeneration from tau decays and tau energy loss for neutrinos with energies above 10^6 GeV, with a particular interest in the higher energy range relevant for RICE and ANITA. Attenuation shadows most of the upward-going solid angle for neutrinos, so we concentrate on incident neutrinos which are nearly horizontal or slightly upward-going. Considering the correct propagation of tau neutrinos is important for a number of reasons. The effective volume for the detection of ν_τ is larger than for the other flavors due to the regeneration effects. The initial interaction happens far outside the detector, but the neutrinos (taus) produced in the neutrino interaction-tau decay cascade interact (decay) inside the detector. This can lead to enhanced event rates for particular energies and trajectories. The regenerated neutrinos and taus contribute, however, at lower energies than the initial ones, so a detailed quantitative analysis is necessary to understand where the regeneration effects are significant. Besides the possible enhancement in the rates, a good discrimination between all the different neutrino flavors is important. The flavor composition of the detected neutrino fluxes could provide a better understanding of the sources of such neutrinos and neutrino properties. The separate identification of each flavor could be important for this purpose [11].

We illustrate our results with a variety of fluxes. We concentrate our analysis on the flux of GZK neutrinos [12]. These are produced in the decay of pions from the interaction of cosmic ray protons with the background microwave photons, so they are a “guaranteed” source. In addition, they are expected to dominate the neutrino flux at energies for which the radio Cherenkov detection methods are most sensitive if the Z burst model discussed below is not an explanation of the highest energy cosmic rays. Detection of GZK neutrinos could be essential for the understanding of very high energy cosmic ray protons. The normalization of the GZK flux is somewhat uncertain. Our results are based on a conservative value, that considers “standard” cosmological evolution [12]. For “strong” source evolution the same general behavior of the flux is valid, but the flux is a factor of 4 higher, leading to higher rates. Other studies [13] obtain fluxes different by up to one order of magnitude. Since the normalization we use is the smallest, our results are conservative and rates could actually be higher.

In order to discuss how results depend on the shape of the initial flux, we also show two generic distributions, $1/E$ and $1/E^2$. The $1/E$ flux describes well the neutrinos from Z burst models [14, 15]. Z burst models could explain the highest energy cosmic rays by extremely high energy neutrinos

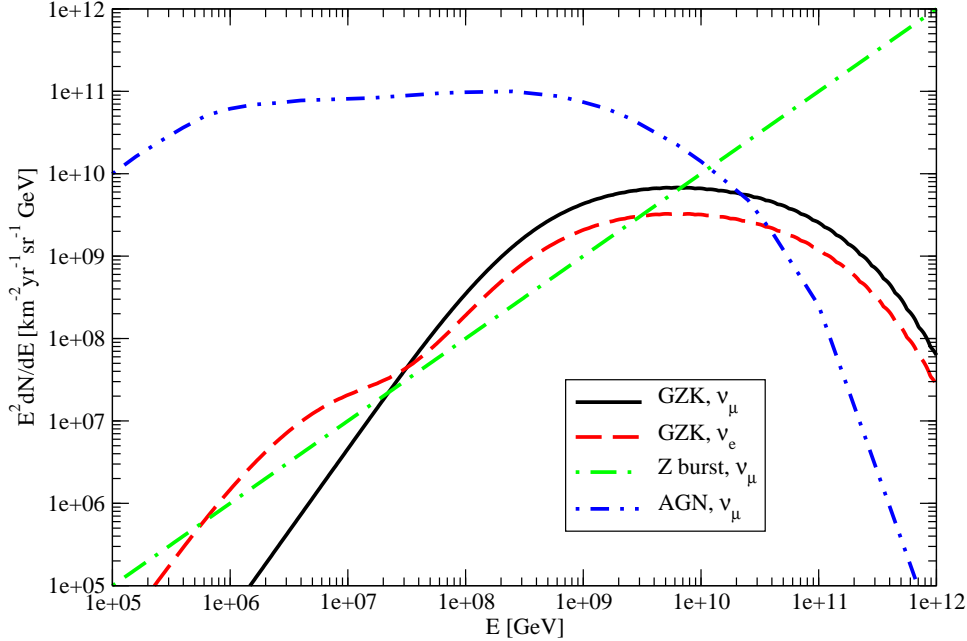


Figure 1: Initial Neutrino Fluxes.

scattering on nearby massive relic neutrinos. We also show results for the neutrino fluxes from AGN's for the model in Ref. [16]. This flux has an approximate $1/E^2$ behavior for $E = 10^6 - 10^9$ GeV, so towards the lower end of that energy range, our $1/E^2$ results apply. All of the fluxes used in our analysis are shown in Fig. 1, except for the $1/E^2$ distribution, which would correspond to just a horizontal line.

In the following section we describe our methods of computing the fluxes of neutrinos and charged leptons after propagation through the Earth. In section 3 we discuss the effect of regeneration and lepton energy loss on the propagation of the initial neutrino fluxes. In section 4 we present our results for the distributions of electromagnetic and hadronic showers from tau decays and neutrino interactions relevant to the different types of experiments. Other recent papers [5, 17] have focused on IceCube detection or on air showers. Related work has been recently presented at ICRC 2003 [18]. Here, we consider IceCube, as well as RICE and ANITA, which also use the ice as detector and have higher energy sensitivities. In the case of ANITA, one has dramatically longer trajectories through the ice to consider.

2 Neutrino and Charged Lepton Propagation

Neutrino attenuation and regeneration are governed by interaction lengths and decay lengths. In Fig. 2, we show the neutrino interaction length (in water equivalent distance), as well as the tau decay length and the effective decay length when one includes tau energy loss in water [19, 20].

The upper curve for the neutrino interaction length is equally applicable to antineutrinos, since at high energies the neutrino and antineutrino cross sections with nucleons are essentially equal because the cross sections are sea quark dominated. The neutral current contribution to the total cross section is about 1/2 of the charged current contribution.

To compare the interaction lengths with physical distances, we note that $D = 2R_{\oplus} \cos \theta \simeq 6 \times 10^8$ cm.w.e. for $\theta = 80^\circ$ and $D \simeq 2 \times 10^7$ cm.w.e. for $\theta = 89^\circ$ where $R_{\oplus} = 6.37 \times 10^8$ cm is the radius of the Earth. Neutrino attenuation is clearly an important effect, even for nearly horizontal incident neutrinos. In the figures below, we mainly show results for a nadir angle of 85° where attenuation and regeneration effects in the propagation of ν_τ 's is in effect without dramatically reducing the flux. We also compare fluxes with those from incident 80° and 89° nadir angles.

The effective decay length of the tau shows that, for energies above about 10^8 GeV, the tau is more likely to interact electromagnetically than to decay [20]. For an initial tau energy of 10^{12} GeV, the average energy just before it decays is a few $\times 10^8$ GeV, depending on the density of the material the tau is passing through. Its effective decay length is of order 50 km in water. We use a density of $\rho = 0.9$ g/cm³ for ice.

For tau neutrinos, we take into account the attenuation by charged current interactions, the shift in energy due to neutral current interactions and the regeneration from tau decay. For tau leptons we consider their production in charged current ν_τ interactions, their decay, as well as electromagnetic energy loss. The tau neutrino and tau fluxes satisfy the following transport equations:

$$\begin{aligned} \frac{\partial F_{\nu_\tau}(E, X)}{\partial X} = & -N_A \sigma^{tot}(E) F_{\nu_\tau}(E, X) + N_A \int_E^\infty dE_y F_{\nu_\tau}(E_y, X) \frac{d\sigma^{NC}}{dE}(E_y, E) \\ & + \int_E^\infty dE_y \frac{F_\tau(E, X)}{\lambda_\tau^{dec}} \frac{dn}{dE}(E_y, E) \end{aligned} \quad (1)$$

$$\frac{\partial F_\tau(E, X)}{\partial X} = -\frac{F_\tau(E, X)}{\lambda_\tau^{dec}(E, X, \theta)} + N_A \int_E^\infty dE_y F_{\nu_\tau}(E_y, X) \frac{d\sigma^{CC}}{dE}(E_y, E) \quad (2)$$

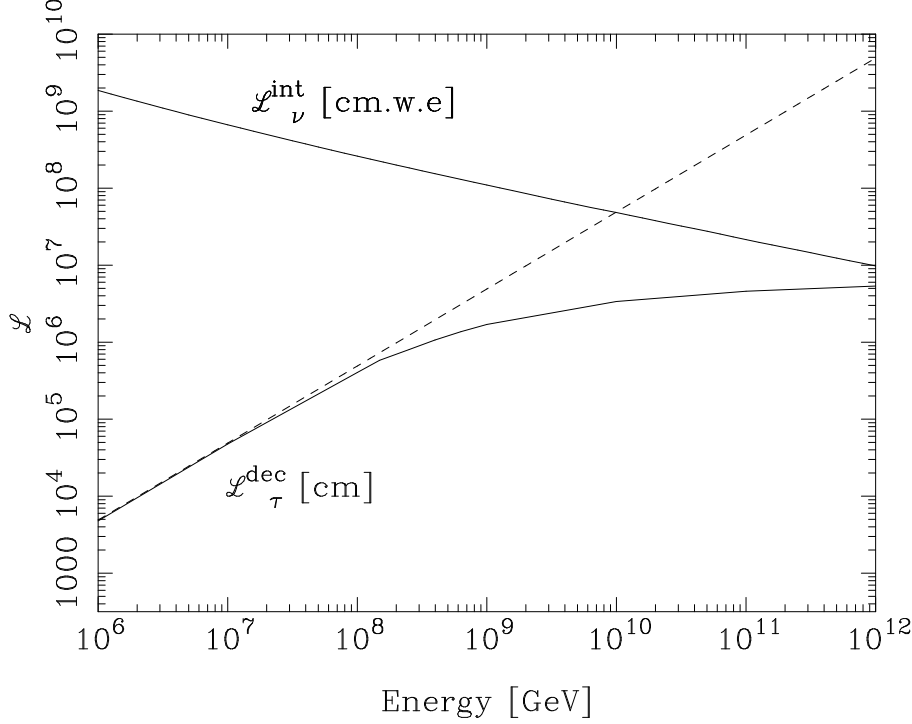


Figure 2: Neutrino interaction length (solid line) and tau effective decay length neglecting energy loss (dashed line) and including electromagnetic energy loss in water (solid line).

$$-\frac{dE_\tau}{dX} = \alpha + \beta E_\tau \quad (3)$$

Here $F_{\nu_\tau}(E, X) = dN_{\nu_\tau}/dE$ and $F_\tau(E, X) = dN_\tau/dE$ are the differential energy spectra of tau neutrinos and taus respectively, for lepton energy E , at a column depth X in the medium defined by

$$X = \int_0^L \rho(L') dL'. \quad (4)$$

We use the average density $\rho(L)$ of the medium along the neutrino path, as given by the Preliminary Earth Model [21]. We note that Antarctica is covered by a sheet of ice with a few km thickness, so that some of the neutrino trajectories can go mostly or even entirely through ice rather than rock. For the neutrino interaction cross-sections we use CTEQ6 parton distribution functions [22] and their extrapolation in the regions of interest to us [19].

The decay length of the tau is $\lambda_\tau^{dec}(E, X, \theta) = \gamma c \tau_\tau \rho$. We use the decay distributions dn/dE written explicitly in Ref. [4], and we approximate the energy distribution of the neutrino interaction process with $d\sigma/dy(E, y) \simeq \sigma(E)\delta(y - \langle y \rangle)$, with $y = (E - E')/E$ for incident neutrino energy E and outgoing lepton energy E' and $\langle y \rangle = 0.2$.

Equation (3) describes the approximate energy loss of the tau. The parameter α is determined by the ionization energy loss and is negligible at high energy. The parameter β is due to radiative energy loss through bremsstrahlung, pair production and photonuclear scattering. The photonuclear scattering becomes dominant at very high energies. As a first approximation we use $\beta = 0.8 \times 10^{-6} \text{ cm}^2/\text{g}$ for the τ energy loss. There is a negligible change (\lesssim a few %) if one uses a more realistic $\beta(E) = (0.16 + 0.069 \log_{10}(E_\tau/\text{GeV})) \times 10^{-6} \text{ cm}^2/\text{g}$ [20] except at very high energies ($E_\tau > 10^{10} \text{ GeV}$), where the flux is extremely low. We use an energy loss parameter $\beta = 7 \times 10^{-6} \text{ cm}^2/\text{g}$ for the muons.

It should be added here that for $\bar{\nu}_e$ the additional scattering on electrons should be considered because of the W boson resonance at $6.3 \times 10^6 \text{ GeV}$. However, this resonance is extremely narrow (narrower than the energy resolution of the experiments) and it contributes a negligible amount to total rates [6, 19].

In [23] it has been pointed out that the secondary fluxes of $\bar{\nu}_e$ and $\bar{\nu}_\mu$ from the tau decays could also have a significant contribution for a flux of mono-energetic neutrinos. In [24] it has been shown however that secondary neutrinos have negligible contribution for large nadir angles (i.e. for $\theta > 60^\circ$) for generic initial neutrino fluxes, $1/E$ and $1/E^2$. The fluxes of secondary neutrinos are described by a transport equation similar to Eq. (1), with the decay distribution dn/dE characteristic to each of the secondary neutrinos and we include them here, even though they are very small.

3 Neutrino and Tau Fluxes

From Eqs. (1,2,3) for τ 's, and from suitably modified equations for muons, we evaluate the charged lepton fluxes at the end of the trajectory of a neutrino incident with nadir angle θ .

For most astrophysical sources, the neutrinos are produced in pion decays, which determine the flavor ratio $\nu_e : \nu_\mu : \nu_\tau$ to be $1 : 2 : 0$. After propagation over very long distances, neutrino oscillations change this ratio to $1 : 1 : 1$

because of the maximal $\nu_\mu \leftrightarrow \nu_\tau$ mixing. For the GZK flux, ν_e and ν_μ incident fluxes are different because of the additional contributions from $\bar{\nu}_e$ from neutron decay and ν_e from μ^+ decays [12]. Because of this, the flavor ratio at Earth is affected by the full three flavor mixing and is different from $1 : 1 : 1$. Given fluxes at the source $F_{\nu_e}^0$, $F_{\nu_\mu}^0$ and $F_{\nu_\tau}^0$, the fluxes at Earth become:

$$F_{\nu_e} = F_{\nu_e}^0 - \frac{1}{4} \sin^2 2\theta_{12} (2F_{\nu_e}^0 - F_{\nu_\mu}^0 - F_{\nu_\tau}^0) \quad (5)$$

$$F_{\nu_\mu} = F_{\nu_\tau} = \frac{1}{2} (F_{\nu_\mu}^0 + F_{\nu_\tau}^0) + \frac{1}{8} \sin^2 2\theta_{12} (2F_{\nu_e}^0 - F_{\nu_\mu}^0 - F_{\nu_\tau}^0) \quad (6)$$

where θ_{12} is the mixing angle relevant for solar neutrino oscillations. We have assumed that θ_{23} , the mixing angle relevant for atmospheric neutrino oscillations, is maximal and θ_{13} is very small, as shown by reactor experiments, as well as atmospheric and solar data. We use the initial GZK flux evaluated by Engel, Seckel and Stanev [12] for standard evolution and we get the fluxes at Earth from the equations (5) and (6). The fluxes of ν_μ and ν_τ are still equal, due to the maximal $\nu_\mu \leftrightarrow \nu_\tau$ mixing. The main effect of the three flavor oscillations is to transform some of the low energy ν_e 's into ν_μ and ν_τ . This could be useful since IceCube has very good sensitivity for detecting tracks, which are enhanced in this case.

To illustrate the effect of the charged lepton lifetime and electromagnetic energy loss in propagation, we begin with muon and tau distributions. Fig. 3 shows the tau and muon distributions for the GZK neutrinos at the end of the trajectory through the Earth with a nadir angle of 85° , with and without taking into account the energy loss of the charged lepton. As noted above, the incident ν_μ and ν_τ fluxes are equal. It is clear from here that the energy loss is extremely important and strongly limits the fluxes at very high energy. Including energy loss, the difference between the τ and μ flux above 10^7 GeV comes from the ν_τ pileup from interaction and regeneration, as well as to the difference in decay length and energy loss for taus and muons. Most of the charged leptons are produced in the last step of neutrino propagation. The muon flux below 10^7 GeV dominates the tau flux because of the much longer decay length of the muon.

Fig. 4 shows the distribution of ν_τ , ν_μ and ν_e fluxes after propagation through the Earth for the same initial flux and angle. For ν_e and ν_μ the transport equations are effectively decoupled from those of the charged leptons and their propagation is given by Eq. (1) in which the last term is not

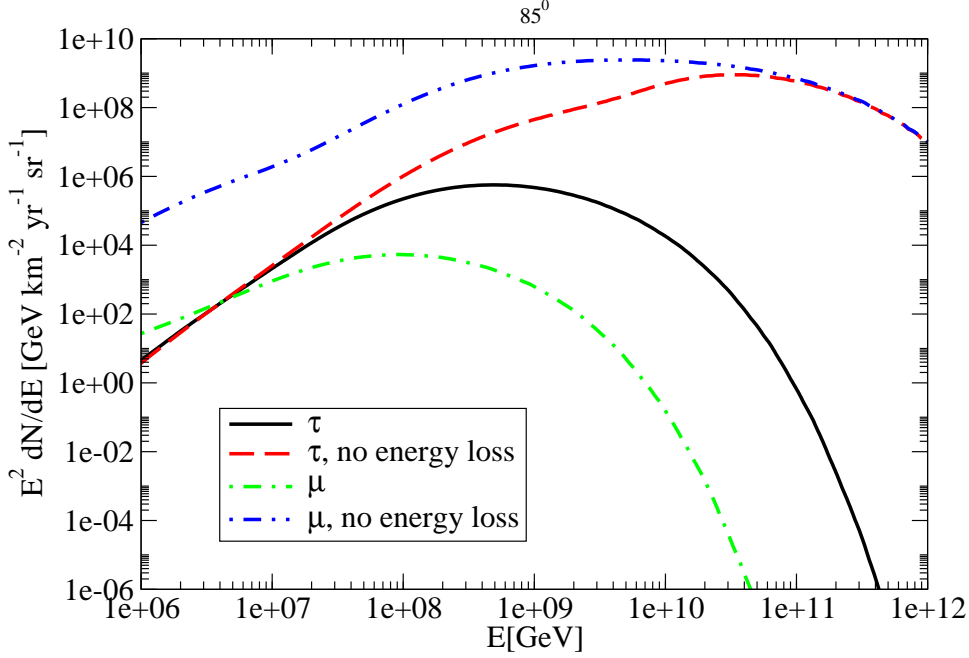


Figure 3: Charged lepton distributions for GZK neutrinos, at a nadir angle of 85° .

present. On the same figure we show the flux of secondary ν_μ neutrinos, which is the same with that of the secondary ν_e . It can be seen that their contribution is negligible, with maximum corrections of the order of a few percent around 10^7 GeV and much smaller for most energies. At larger nadir angles, the secondary neutrino contribution will be an even smaller fraction of the ν_e and ν_μ fluxes. At smaller nadir angles, the secondary flux will be a larger percentage of the overall neutrino flux, but the flux will become more strongly attenuated.

Fig. 5 shows the same ν_τ distribution as in the previous figure, together with the distributions obtained if energy loss of tau leptons or the shift in energy due to neutral current is not included in the propagation. Electromagnetic energy loss is extremely important at energies above 10^8 GeV and this effect causes strong suppression of the neutrino fluxes at very high energy. If the tau would not lose energy in its propagation, the regeneration effect would be much bigger at high energy. The $\nu_\tau \rightarrow \tau \rightarrow \nu_\tau$ regeneration is a significant effect for energies between 10^6 and 10^8 GeV, as can be seen

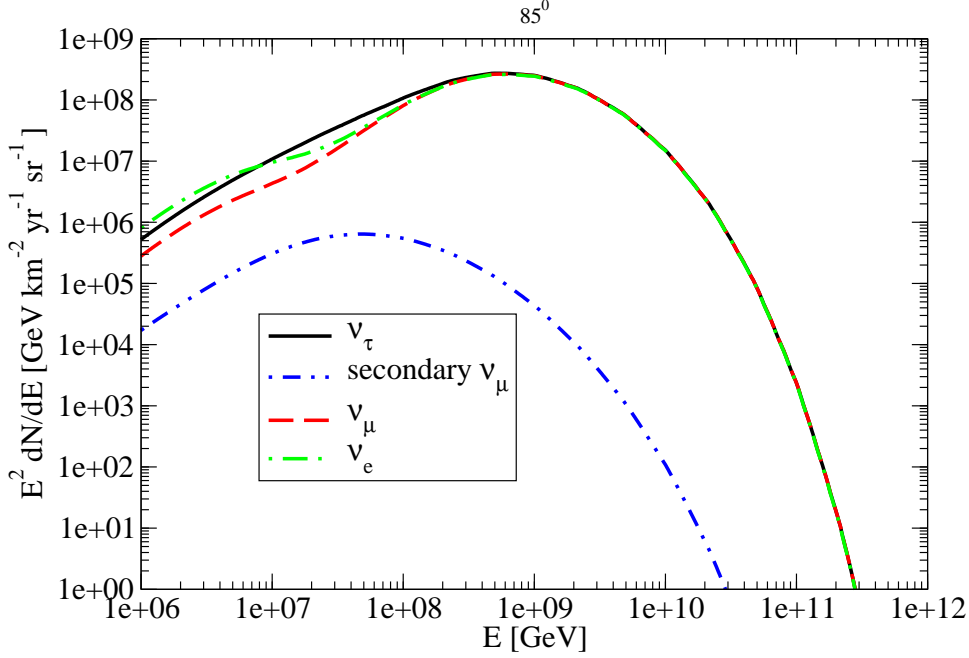


Figure 4: Neutrino distributions for GZK neutrinos, at a nadir angle of 85° .

more clearly in Fig. 7. The neutral current interactions of the neutrinos are also very important, as can be seen in Fig. 5 by comparing the flux of ν_τ after correct propagation with a simple attenuation with $\exp(-D/\mathcal{L}_{int}^\nu(E))$ for column depth D and interaction length \mathcal{L} evaluated using the charged current cross section. The difference can be as large as two orders of magnitude at very high energy.

Fig. 6 shows the τ and ν_τ distributions for the same initial neutrino flux, but for different nadir angles. As the neutrinos pass through more matter, the regeneration effects become relatively more important, but the overall fluxes get significantly attenuated. At a nadir angle of 80° the Earth is already opaque to neutrinos with energies above 10^{10} GeV.

Fig. 7 shows the ratio of the tau neutrino flux after propagation to incident tau neutrino flux, for 89° , 85° and 80° . This ratio illustrates a combination of the regeneration of ν_τ due to tau decay and the attenuation of all neutrino fluxes. For 89° , where both the total distance and the density are smaller, the attenuation is less dramatic, and the flux can be significant even at high energy. The regeneration in this case can add about 25% corrections

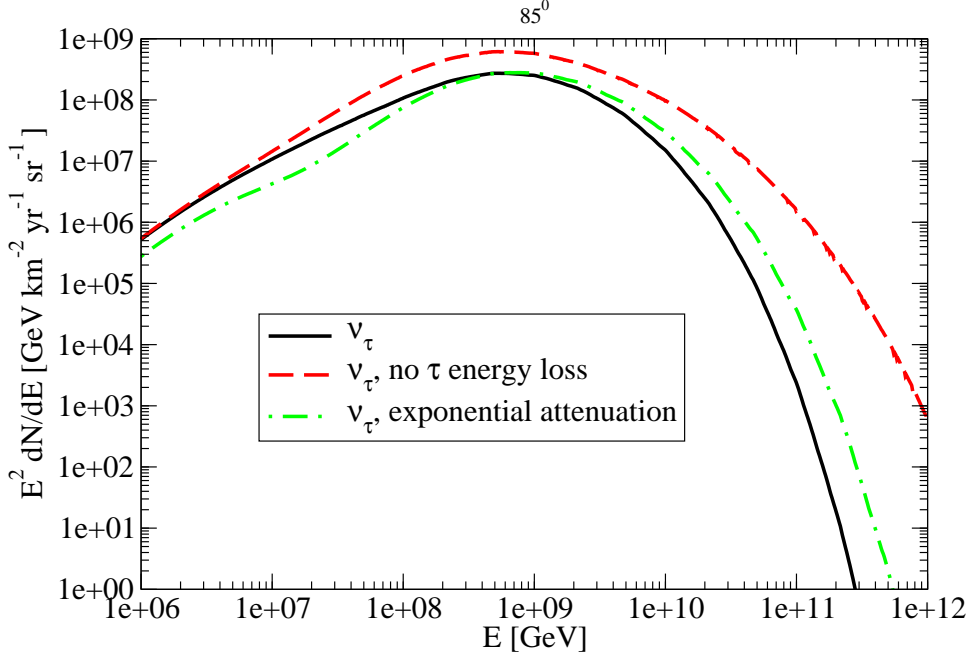


Figure 5: Tau neutrino distributions for the GZK flux, at a nadir angle of 85° .

at energies between 10^7 and 10^8 GeV. For 85° the relative enhancement is around 80% and peaked at slightly lower energies, while at 80° it is almost a factor of 3 at low energy. At 80° , however, the flux is very strongly attenuated for energies above a few $\times 10^7$ GeV.

It is already clear from Fig. 7 that the total rates will be dominated by the nearly horizontal trajectories that go through a small amount of matter. The largest pileups occur when the trajectory of the neutrino passes through a larger column depth. For the higher energies relevant to RICE and ANITA, this doesn't translate to higher fluxes of ν_τ 's. Attenuation is the main effect at those energies. Rates can get significant enhancements at low energies where the regeneration from tau decays adds an important contribution even for longer trajectories.

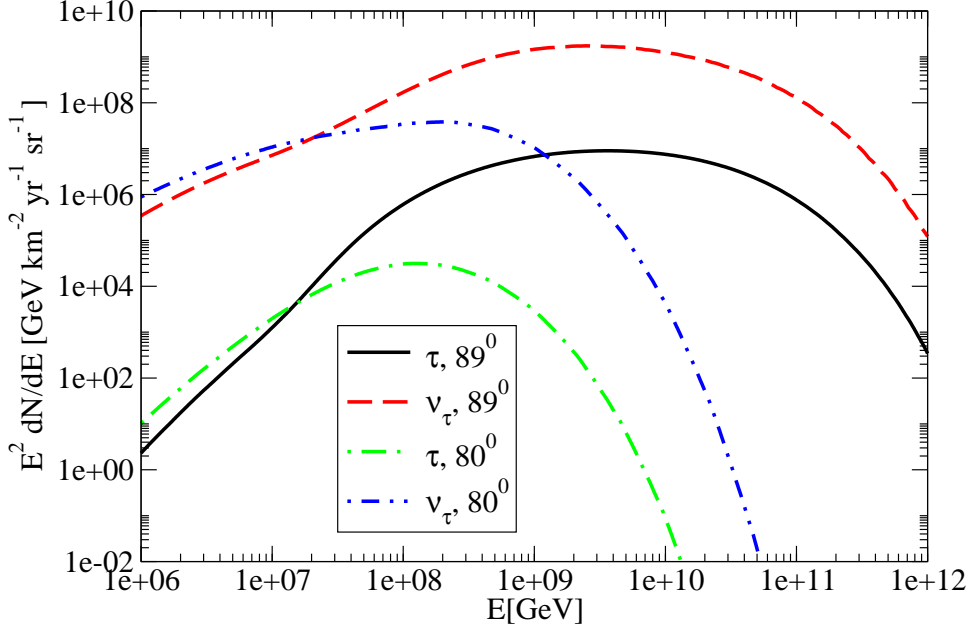


Figure 6: The τ and ν_τ distributions for GZK neutrinos for different nadir angles.

4 Showers

The above distributions illustrate the effects of the propagation through matter on the initial neutrino fluxes. We now turn to the experimentally relevant observables, which are the showers.

We consider hadronic showers produced in ν_τ interactions, as well as electromagnetic and hadronic showers from τ decays in ice. All other flavors of neutrinos will contribute to the hadronic showers, while ν_e will also contribute to electromagnetic showers. The shower distributions will be different for each type of experiment, depending on the detector setup.

We start by considering contributions to electromagnetic and hadronic showers in a depth of ~ 1 km of ice, relevant for experiments like IceCube and RICE.

We use Eqs. (1-3) and the corresponding ones for e and μ flavors to obtain the tau and neutrino distributions ($F_\tau(E_\tau)$ and $F_\nu(E_\nu)$) after propagation up to the last few km of ice. We then estimate the shower distributions that are produced over the distance $d \sim \text{few km}$. The contributions of neutral

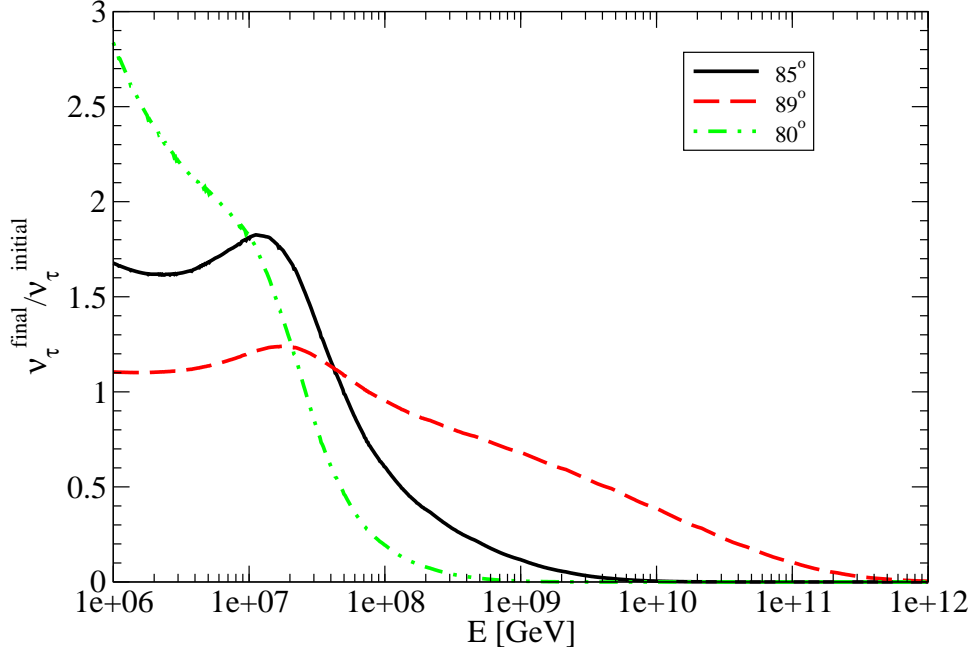


Figure 7: Ratio $\nu_\tau^{\text{final}}/\nu_\tau^{\text{initial}}$ for GZK neutrinos, at nadir angles of 80° , 85° and 89° .

currents and regeneration over a few kilometers is small and here we neglect them for the last part of the trajectory, which is where the showering takes place. This can no longer be done when showers are detected over long distances, as will be the case for ANITA.

There are two contributions to electromagnetic showers from tau decays. One is from the decay of the taus produced outside the detector that decay electromagnetically inside the detector, giving “lollipop” events in IceCube and electromagnetic showers in RICE. The distribution of these showers is given as a function of the energy of the electron produced in the decays by:

$$F_{sh,\tau}^{em,1}(E_e) = \int_{E_e}^{E_{max}} dE_\tau \int_0^{d\rho} dx F_\tau(E_\tau) e^{-x/\lambda_\tau^{dec}(E_\tau e^{-\beta x})} \frac{1}{\lambda_\tau^{dec}(E_\tau e^{-\beta x})} \frac{dn_{\tau \rightarrow e}}{dE_e}(E_\tau e^{-\beta x}, E_e) \quad (7)$$

where $F(E) \equiv dN/dE$ is the flux of taus just before the final column depth d in ice and $\rho = 0.9 \text{ g/cm}^3$ is the density of ice. For negligible energy loss (which is a very good approximation below 10^9 GeV in 1 km of ice) this

becomes:

$$F_{sh,\tau}^{em,1}(E_e) = \int_{E_e}^{E_{max}} dE_\tau F_\tau(E_\tau) \left(1 - e^{-d\rho/\lambda_\tau^{dec}(E_\tau)}\right) \frac{dn_{\tau \rightarrow e}}{dE_e}(E_\tau, E_e) \quad (8)$$

The other contribution comes from the taus that are produced and decay electromagnetically inside the detector. In IceCube these correspond to “double bang” events. The distribution is obtained from:

$$\begin{aligned} F_{sh,\tau}^{em,2}(E_e) &= \int_0^{d\rho} dx \int_x^{d\rho} dy \int_{E_e}^{E_{max}} dE_{\nu_\tau} \int_{E_e}^{E_{\nu_\tau}} dE_\tau F_{\nu_\tau}(E_{\nu_\tau}) \\ &\quad e^{-x N_A \sigma^{CC}(E_{\nu_\tau})} N_A \frac{d\sigma^{CC}}{dE_\tau}(E_{\nu_\tau}, E_\tau) \\ &\quad e^{-y/\lambda_\tau^{dec}(E_\tau e^{-\beta y})} \frac{1}{\lambda_\tau^{dec}(E_\tau e^{-\beta y})} \frac{dn_{\tau \rightarrow e}}{dE_e}(E_e, E_\tau e^{-\beta y}) \end{aligned} \quad (9)$$

When energy loss is negligible, this becomes:

$$\begin{aligned} F_{sh,\tau}^{em,2}(E_e) &= \int_{E_e}^{E_{max}} dE_{\nu_\tau} \int_{E_e}^{E_{\nu_\tau}} dE_\tau F_{\nu_\tau}(E_{\nu_\tau}) N_A \frac{d\sigma^{CC}}{dE_\tau}(E_{\nu_\tau}, E_\tau) \frac{dn_{\tau \rightarrow e}}{dE_e}(E_e, E_\tau) \\ &\quad \left(\frac{1}{N_A \sigma^{CC}(E_{\nu_\tau}) + 1/\lambda_\tau^{dec}(E_\tau)} \left(1 - e^{-d\rho(N_A \sigma^{CC}(E_{\nu_\tau}) + 1/\lambda_\tau^{dec}(E_\tau))}\right) - \right. \\ &\quad \left. \frac{1}{N_A \sigma^{CC}(E_{\nu_\tau})} e^{-d\rho/\lambda_\tau^{dec}(E_\tau)} \left(1 - e^{-d\rho N_A \sigma^{CC}(E_{\nu_\tau})}\right) \right) \end{aligned} \quad (10)$$

The main source of electromagnetic showers comes from the ν_e charged current interactions given by:

$$F_{sh,\nu}^{em} = \int_{E_e}^{E_{max}} dE_\nu F_\nu(E_\nu) (1 - e^{-d\rho N_A \sigma^{CC}(E_\nu)}) \frac{1}{\sigma^{CC}(E_\nu)} \frac{d\sigma^{CC}}{dE_e}(E_\nu, E_e) \quad (11)$$

Hadronic showers from tau decays are given by Eqs.(8) with the electron replaced by hadrons.

The hadronic showers from ν_τ interactions are given by:

$$F_{sh,\nu}^h = \int_{E_h}^{E_{max}} dE_\nu F_\nu(E_\nu) (1 - e^{-d\rho N_A \sigma(E_\nu)}) \frac{1}{\sigma(E_\nu)} \frac{d\sigma}{dE_h}(E_\nu, E_h). \quad (12)$$

In Eq. (12), σ is the total cross section and the hadronic energy comes from the energy transfer to the target nucleus.

Hadronic showers are also produced in ν_μ and ν_e neutral current and charged current interactions. These are also obtained from Eq. (12), using the corresponding fluxes.

We briefly describe below all types of interactions and their signatures in the various experiments. We then show shower distributions relevant in each case.

4.1 Showers in kilometer size detectors: IceCube, RICE

A km^3 Cherenkov detector in ice, IceCube [7] has sensitivity to high energy neutrinos up to $\sim 10^8 - 10^9$ GeV, the energy range where distinguishing the effects of tau neutrinos from muon and electron neutrinos could be possible.

Neutral current interactions of all types of neutrinos produce hadronic showers. Charged current interactions of ν_e contribute to both hadronic and electromagnetic showers. It is likely that IceCube would observe a big shower with the total energy of the incoming neutrino rather than be able to separate the two components (hadronic and electromagnetic). Charged current interactions of ν_μ give a hadronic shower and a muon. The muon track is the main signal in IceCube, so these events are easily identifiable, containing a shower and a long track emerging from it. At high energies however, the same signal could be produced by a ν_τ interaction, since the decay length of the tau becomes longer than the size of the detector for energies above a few $\times 10^7$ GeV.

Charged current ν_τ interactions can have very different signatures depending on energy. At 10^6 GeV, the tau decay length is ~ 50 m, and the shower (hadronic or electromagnetic) from the tau decay cannot be separated from the hadronic shower from the initial ν_τ interaction. At a few times 10^6 GeV the range of the tau becomes a few hundred meters and can give the characteristic signal of the “double bang” events [25]. These are events where the shower from the neutrino interaction and the shower from the tau decay can be separated and are both observed in the detector, together with the tau track. At a few $\times 10^7$ GeV the tau decay length is already longer than 1 km, and the taus look like muons. What is seen is the shower from the neutrino interaction and then a track.

Taus produced in neutrino interactions outside the detector can generate “lollipop” events. The initial shower from the neutrino interaction that produces the tau is missed and what is seen is the track of the tau and the shower from its decay that IceCube can identify as electromagnetic or hadronic from

the existence of muon tracks in the shower.

RICE [9] uses dipole antennas in the Antarctic ice to measure radio frequency Cherenkov radiation from high energy showers. For energies around 10^9 GeV the effective volume of the detector is $\sim 15 \text{ km}^3\text{sr}$. At present, RICE limits the fluxes of downward ν_e with energies between $\text{few} \times 10^7$ and 10^{12} GeV [9]. Interactions modeled by a Monte Carlo at an energy of 10^9 GeV are detected from within a depth of 1 km from the surface and out to a radial distance of about 4 km. The effective volume of the detector has a strong dependence on energy below 10^9 GeV. Hadronic and electromagnetic showers can be separately identified, with somewhat different effective volumes, depending on energy. The RICE experiment can therefore measure electromagnetic showers from ν_e interactions, hadronic showers from the charged and neutral current interactions of all flavors of neutrinos and electromagnetic and hadronic showers from tau decays.

Fig. 8 shows the electromagnetic shower distributions at a nadir angle of 85° . In the absence of the tau neutrinos, only ν_e interactions lead to electromagnetic showers. These $\nu_e \rightarrow e$ CC conversions still dominate at high energies, even when tau neutrinos produce tau leptons that decay electromagnetically. At lower energies however, the taus add a significant contribution to the electromagnetic shower signal. Tau decays give their most important relative contribution to electromagnetic showers at electron energies of a $\text{few} \times 10^7 \text{ GeV}$. These decays are separated in “double bang” and “lollipop” events on the same plot. It can be seen that the contribution of the “double bang” is relatively small. They do not contribute significantly to total event rates, but even in very small numbers they are important as a characteristic signature for taus. Secondary ν_e interactions also produce electromagnetic showers, but it can be seen that their contribution is very small.

Fig. 9 shows the hadronic shower distributions. The features seen in the neutrino fluxes are recovered in the hadronic showers as well. The shower rates from ν_τ , ν_μ and ν_e are nearly identical at shower energies above 10^8 GeV. The tau neutrino pileup is important below 10^8 GeV. Between 10^7 and 10^8 GeV tau decays give the main contribution to the hadronic shower rate. Showers from ν_e and ν_μ secondary neutrinos are also shown and their contribution is negligible.

Fig. 10 shows the ratio of the electromagnetic shower rates at nadir angle 85° in the presence and absence of oscillations for the GZK and Z burst neutrino fluxes. This ratio illustrates the effect of the oscillations on the signal and in particular the possible enhancements due to tau pileup. In absence

Electromagnetic showers

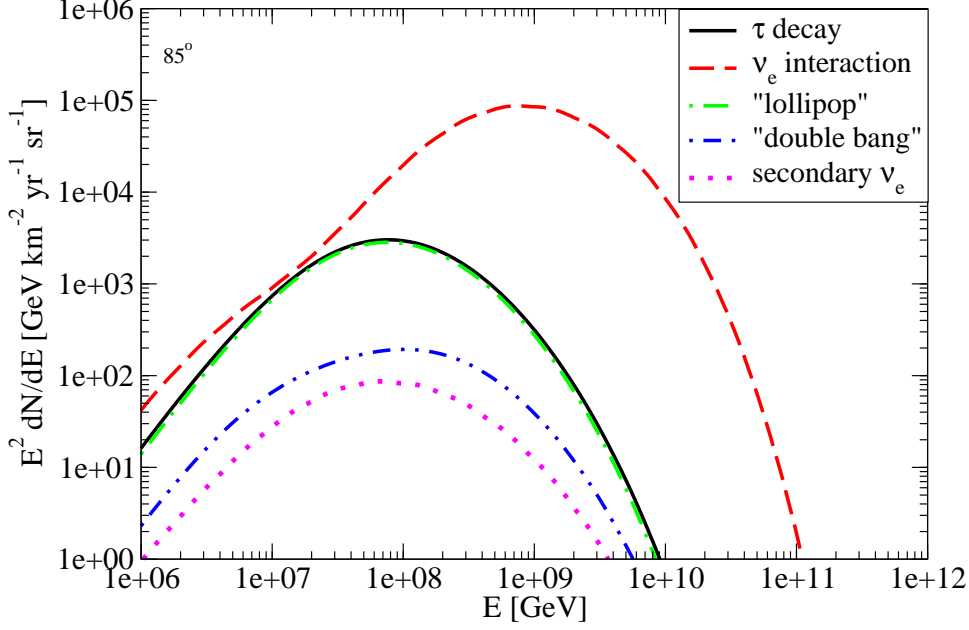


Figure 8: Electromagnetic shower distributions for GZK neutrinos, at a nadir angle of 85° for a km size detector. The τ decay curve is the sum of the lollipop and double bang curves.

of oscillations, the only contribution to electromagnetic showers comes from ν_e interactions. In the presence of $\nu_\mu \rightarrow \nu_\tau$ oscillations, electromagnetic decays of taus from tau neutrinos add significant contributions to these rates at energies below 10^8 GeV. In the same time, for the GZK flux, $\nu_e \rightarrow \nu_{\mu,\tau}$ oscillations reduce the number of ν_e 's at low energy, such that below a few $\times 10^6$ GeV there are fewer electromagnetic showers than in the absence of oscillations.

Fig. 11 shows the ratio of the hadronic shower distributions in presence or absence of oscillations for the same fluxes and nadir angle. Without oscillations, the hadronic showers come from ν_e and ν_μ interactions. In presence of oscillations ν_τ and the ν_e and ν_μ secondaries from tau decay contribute as described above. For hadronic showers the enhancement due to the presence of ν_τ is $\sim 50\%$ at energies of a few $\times 10^7$ GeV. For hadrons there is also some small enhancement for shower energies between 10^8 and 10^9 GeV, which is

Hadronic showers

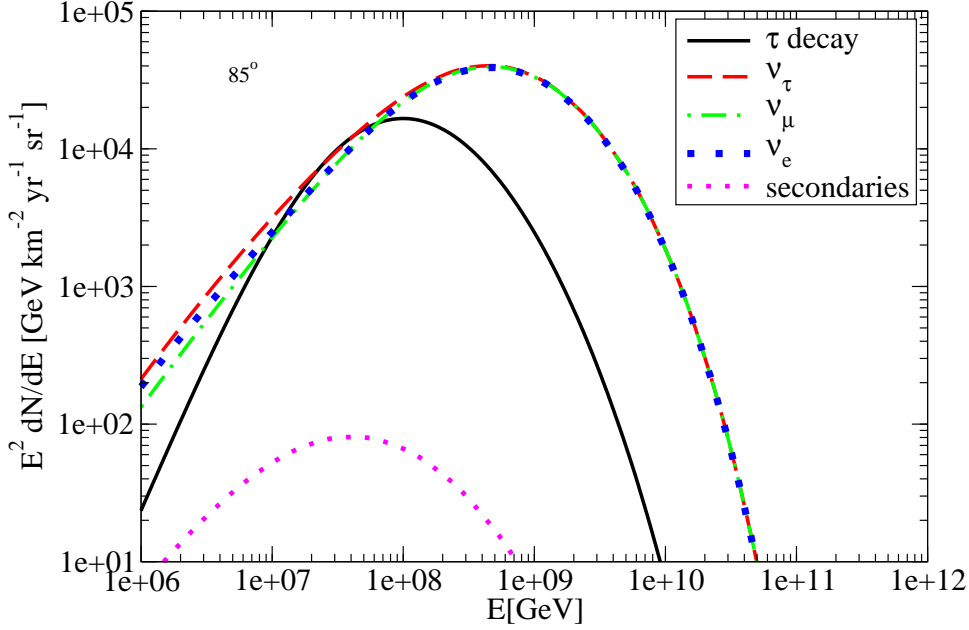


Figure 9: Hadronic shower distributions for GZK neutrinos, at a nadir angle of 85° for a km size detector.

not present for the electromagnetic showers.

The tau contribution can be even more clearly seen if some of the other flavors can be separately identified. As previously discussed, IceCube can identify showers from ν_μ and ν_τ charged current interactions by the μ or τ tracks that emerge and exit the detector. Once these can be removed, what remains are hadronic showers from neutral current interactions of all flavors of neutrinos, ν_e CC interactions in the detector, as well as the hadronic showers from τ decays in the detector (both from taus produced within the detector and from taus produced outside the detector that propagate in and then decay). The enhancement in the ratio is even higher in this case, about 80%.

Fig. 12 also shows the hadronic shower distributions for GZK neutrinos, but at a nadir angle of 89° . As expected, there are more showers for this distance than for the longer one, but the relative contribution of the tau is smaller in this case. This is because both the attenuation and the regeneration effects are much smaller for smaller column densities.

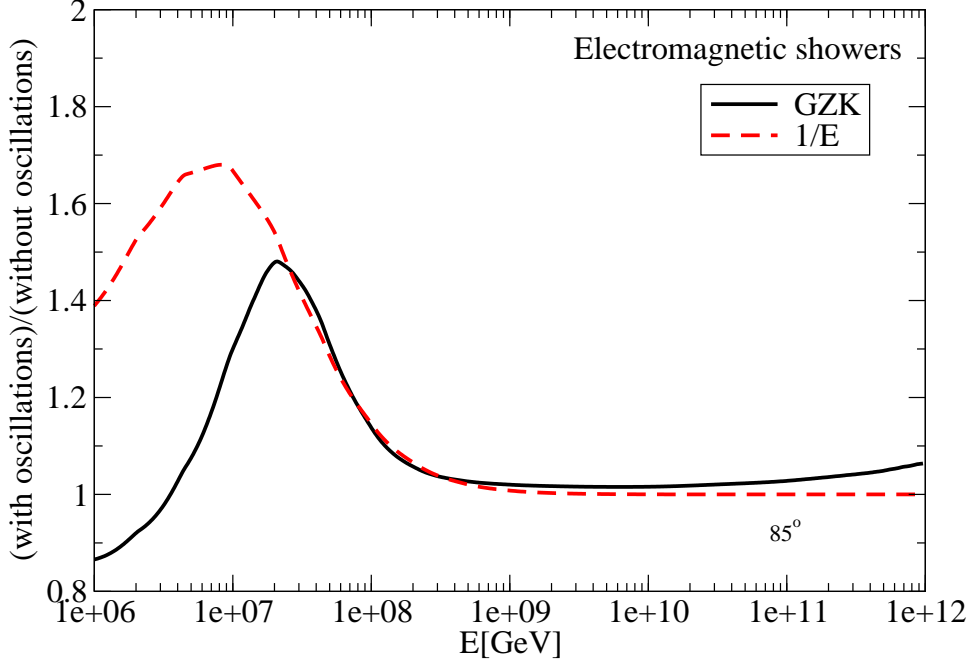


Figure 10: Ratio of electromagnetic shower rates in the presence and absence of $\nu_\mu \rightarrow \nu_\tau$ oscillations for GZK and $1/E$ neutrino spectra for nadir angle 85° for a km size detector.

The experimental angular resolution for high energy showers is about 10° to 25° . Averaging over such angles the effect of the pileup is somewhat reduced (to $\sim 10\%$ of the event rate), since total rates are dominated by the trajectories that go through a small amount of matter. However, rates can get significant enhancements at low energies where the regeneration from tau decays adds an important contribution even for longer trajectories. Consequently, an experiment with low energy threshold has a better chance of detecting the effect. IceCube has a low energy threshold and an energy resolution of $\sim 10\%$, so it is in a good position to look for pileup effects, given a high enough neutrino flux.

The same general features remain true for different initial fluxes. However, the energy distributions are different for each and the enhancement due to regeneration appears at somewhat different energies. The regeneration effects are also smaller for the fluxes steeper at high energy. For example, from Figs. 10 and 11 it can be seen that for the $1/E$ flux, predicted, for

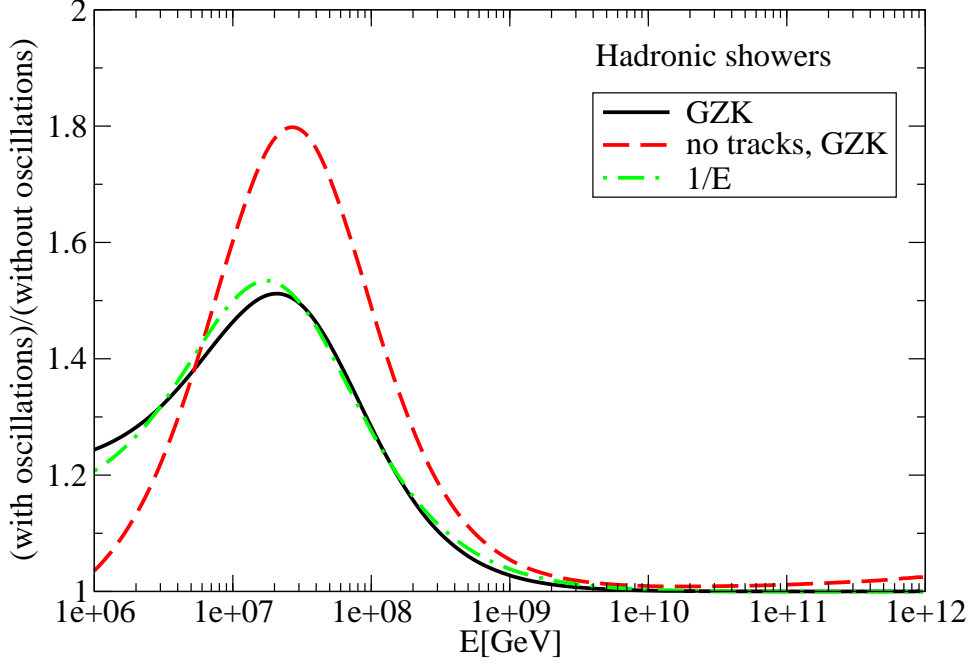


Figure 11: Ratio of hadronic shower rates in the presence and absence of $\nu_\mu \rightarrow \nu_\tau$ oscillations for GZK and $1/E$ fluxes for nadir angle 85° for a km size detector.

example, for Z burst (ZB) models [14], the pileup is slightly bigger, but at a lower energy than for the GZK neutrino flux. This is just as expected, because the GZK flux is steeper at higher energy, but does not fall as rapidly at intermediate energies.

Fig. 13 shows the electromagnetic shower distributions for a $1/E$ flux, for example predicted for Z burst and for a $1/E^2$ generic flux for a nadir angle of 85° . The $1/E^2$ distribution has a normalization of $10^{10} \text{ GeV}^{-1} \text{ km}^{-2} \text{ yr}^{-1} \text{ sr}^{-1}$, about an order of magnitude below the present AMANDA limit [26]. For the ZB flux the normalization is $1 \text{ GeV}^{-1} \text{ km}^{-2} \text{ yr}^{-1} \text{ sr}^{-1}$ up to $2.5 \times 10^{12} \text{ GeV}$. Above this energy the flux is cut off and drops as $1/E^3$. The steepness of the $1/E^2$ flux results in a small pileup and thus the relative contribution of taus is much smaller in this case. Fig. 14 shows the same shower distributions for a nadir angle of 89° . Like for the GZK flux, the attenuation in this case is smaller than for 85° , particularly at high energy. The effect of attenuation at high energy is striking especially for the Z burst flux. At 85° there is

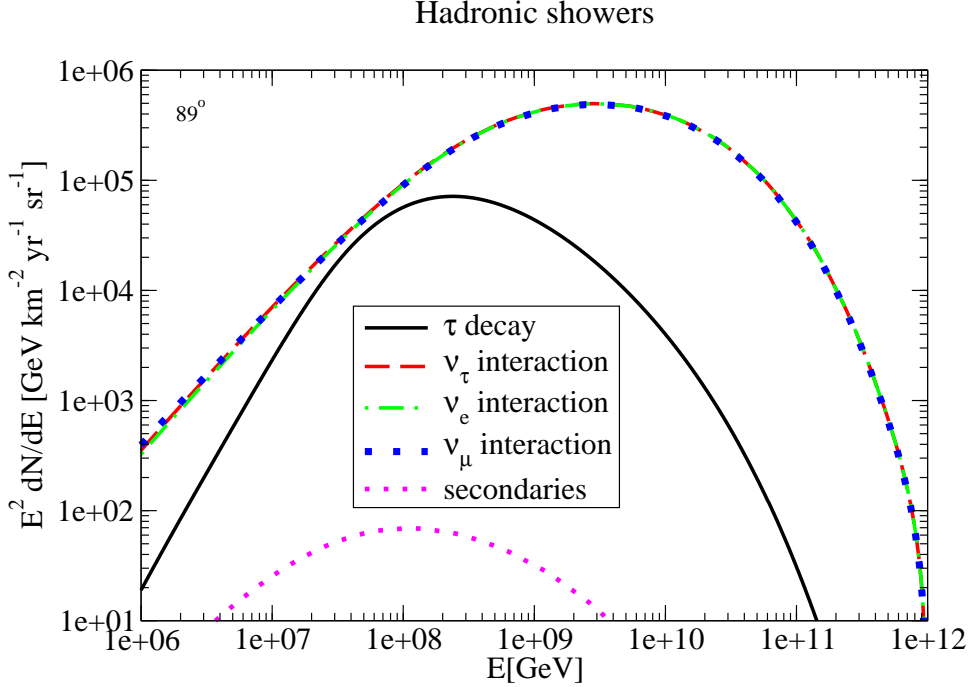


Figure 12: Hadronic shower distributions for GZK neutrinos, at a nadir angle of 89° for a km size detector.

almost no flux left at energies above 10^{10} GeV, while at 89° the neutrino flux is almost unattenuated and still has the $1/E$ shape, being orders of magnitude higher than for the longer pathlength. However, the effects of regeneration become smaller for 89° even for the less steep Z burst flux. It can be clearly seen that, depending on the energy threshold of the detectors, the contribution to event rates comes from different trajectories. At high energies the paths that go through the material with small column density will dominate event rates. However, at energies below 10^8 GeV trajectories that go through 10-15 times more material can contribute equally due to the pileup and additional tau decays.

Fig. 15 shows the hadronic shower distributions for the fluxes used in the previous figures, for a nadir angle of 85° . The energy distribution of the hadronic showers is different from that of electromagnetic ones due to the different decay distributions. Taus decay mostly to hadrons and these hadrons carry most of the energy of the taus. Consequently, the tau contribution to hadronic showers is much higher, bigger than the ν_τ contribution at energies

Electromagnetic showers

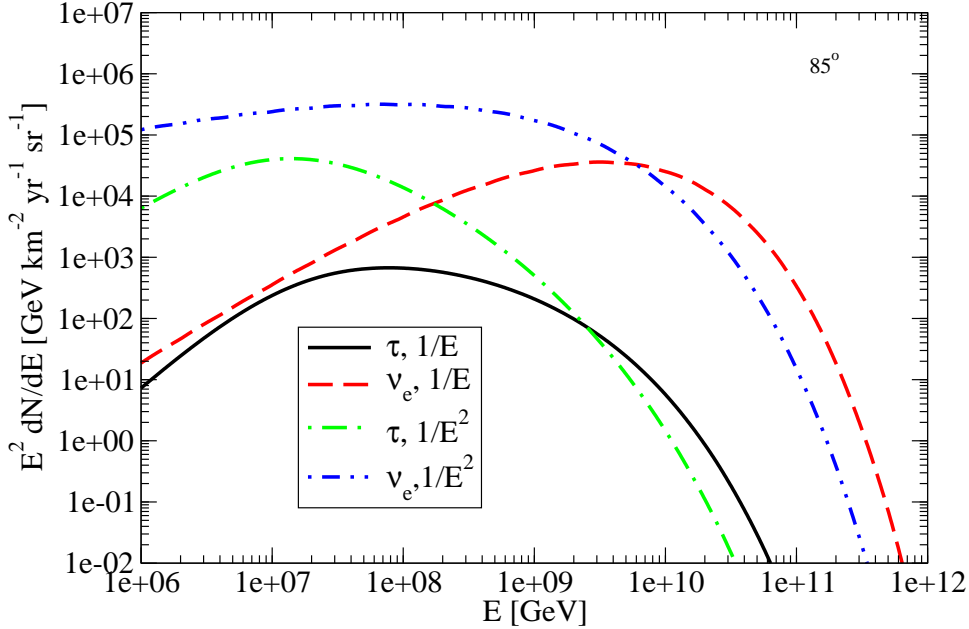


Figure 13: Electromagnetic shower distributions for nadir angle 85° for $1/E$ and $1/E^2$ characteristic fluxes for a km size detector from ν_e interactions and from τ decays.

around a few $\times 10^7$ GeV, and extends to higher energies.

Fig. 16 shows the electromagnetic distributions for the AGN flux in [16] for nadir angles of 85° and 89° . This flux is also steep at high energy and consequently the regeneration effects are small. The relative contribution of the taus is bigger for 85° , but the overall rates are higher for 89° .

The energy threshold of RICE is high and for the energies where the experiment has good sensitivity the ν_τ enhancement is limited by the long lifetime of the tau lepton and by its energy loss, such that it cannot be observed. We want to investigate if this remains true in the case of ANITA, which has a much larger effective volume and consequently has the potential to detect many more tau's decaying over long trajectories.

Electromagnetic showers

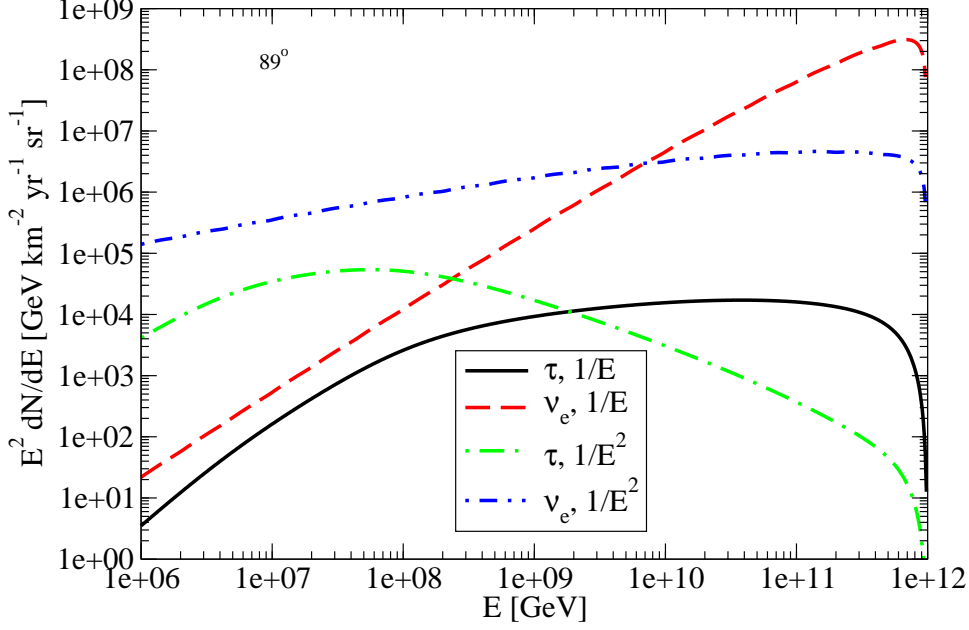


Figure 14: Electromagnetic shower distributions for nadir angle 89° for $1/E$ and $1/E^2$ characteristic fluxes for a km size detector.

4.2 Showers in ANITA

The ANITA experiment also uses the ice as a neutrino converter [10]. The long duration balloon missions will monitor the ice sheet from 40 km in altitude to a horizon approaching 700 km for refracted radio frequency signals with an effective telescope area of 1M km^2 . The geometry of the experiment is rather complicated, as it has to take into account the Cherenkov angle of the radio emission with respect to the particle trajectory, its refraction at the ice surface and the position of the balloon. The huge volume covered gives ANITA remarkable sensitivity for detecting very high energy neutrinos. While IceCube and RICE can only detect showers produced in a km^3 volume, ANITA can detect all the showers produced over long distances in ice.

For example, for a nadir angle of 89° , the entire trajectory (~ 222 km) of the neutrino is in ice, at less than 1 km depth, and all showers produced over this distance can be observed. For a nadir angle of 85° , observable showers (at less than 1 km depth) could be produced over a distance of ~ 12 km.

Hadronic showers

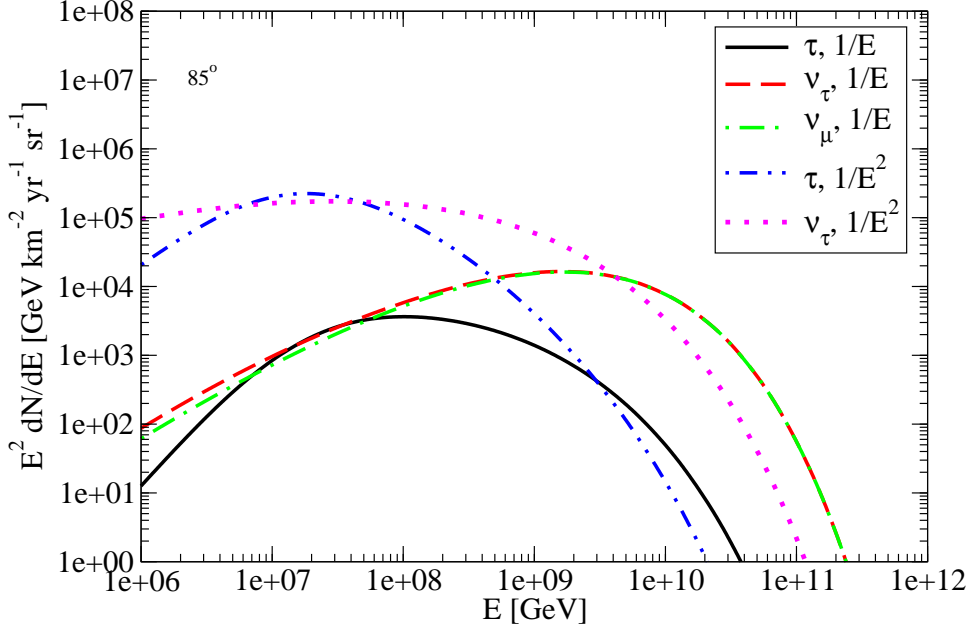


Figure 15: Hadronic shower distributions for nadir angle 85° for $1/E$ and $1/E^2$ characteristic fluxes for a km size detector from neutrino interactions and tau decays. The ν_e distributions are identical to the ν_μ distributions. For the $1/E^2$ flux all neutrinos distributions are almost the same.

Given the very large detector area, a trajectory is not fully defined by the nadir angle of the incident neutrino at the entrance point, one also needs the position of the entrance/exit point with respect to the icecap and the balloon. The trajectories that maximize the path through ice, rather than the ones that combine ice and rock, are the ones likely to dominate event rates because of the much smaller attenuation. Those going through more rock give larger *relative* enhancements due to regeneration. They could in principle contribute as much as the others in the region where the regeneration is effective.

As previously discussed, due to the showering over entire trajectories, we can no longer use Eq. (8-12), but rather we have to combine the propagation and showering from the beginning in order to correctly take into account neutral current interactions, energy loss of tau leptons and neutrino regeneration

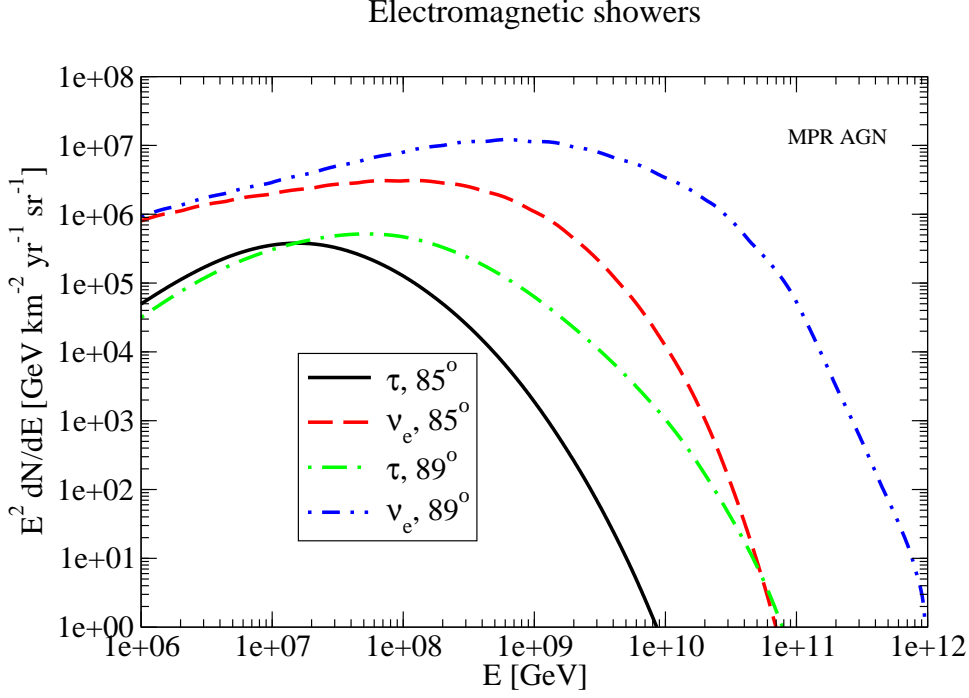


Figure 16: Electromagnetic shower distributions for the MPR AGN model [16] for a km size detector.

from tau decay.

Fig. 17 shows the electromagnetic shower distributions for the GZK and ZB initial fluxes over a trajectory of 222 km in ice. Qualitatively, these are similar to the showers obtained in kilometer size detectors for the same trajectory. However, in this case the rates are larger by up to three orders of magnitude, depending on energy, due to the much larger surface of the detector. The energy distribution is somewhat different, being more spread out toward higher energies. Due to the longer detectable pathlength, higher energy taus, with decay length much longer than 1 km, can now decay producing observable showers.

Fig. 18 shows the hadronic shower distributions for the same initial fluxes and trajectory. The regeneration of the ν_τ neutrinos in this case is very small and ν_μ distributions are almost the same as the ν_τ ones. For the ZB flux, the ν_e distribution is the same as for ν_μ , while for the GZK neutrinos it is different due to the difference in the initial fluxes.

Electromagnetic showers

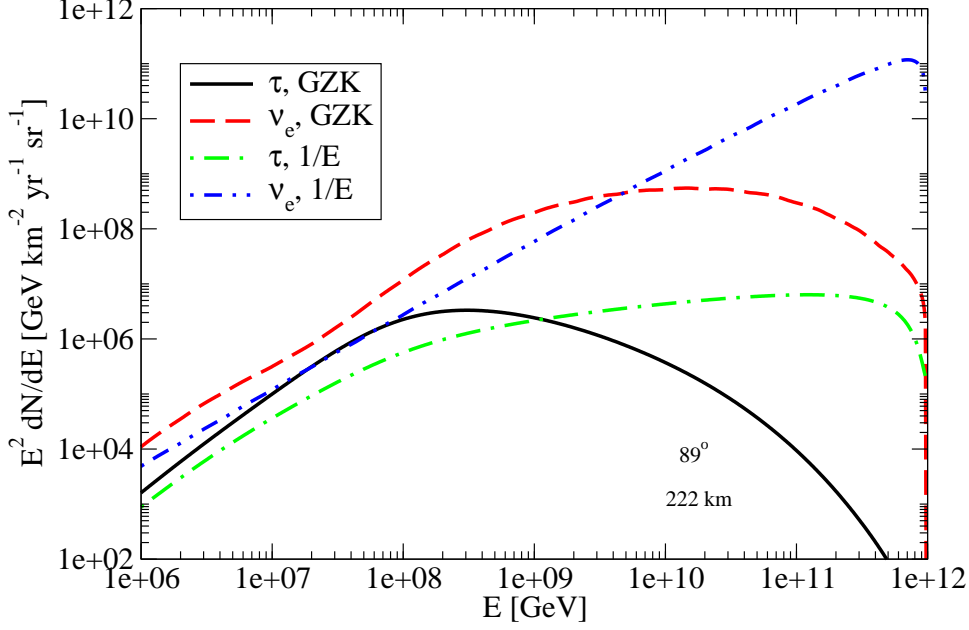


Figure 17: Electromagnetic shower distributions for detection over 222 km of ice.

Fig. 19 shows the ratio of electromagnetic and hadronic shower rates in the presence and absence of $\nu_\mu \rightarrow \nu_\tau$ oscillations corresponding to the distributions in the previous figures. The maximum enhancement due to the presence of ν_τ is about 40% at this angle, as expected since this trajectory has low column density. However, as previously discussed, the enhancement occurs in a larger energy range and it peaks at higher energy than in the case of a small size detectors. In 1 km only taus with energies below a few $\times 10^7$ GeV have a significant probability to decay, while much higher energy taus can decay over the total distance of more than 200 km.

5 Conclusions

We have studied in detail the propagation of all flavors of neutrinos with very high energy ($E \geq 10^6$ GeV) as they traverse the Earth. Because of the high energies, we have limited our consideration to nadir angles larger than

Hadronic showers

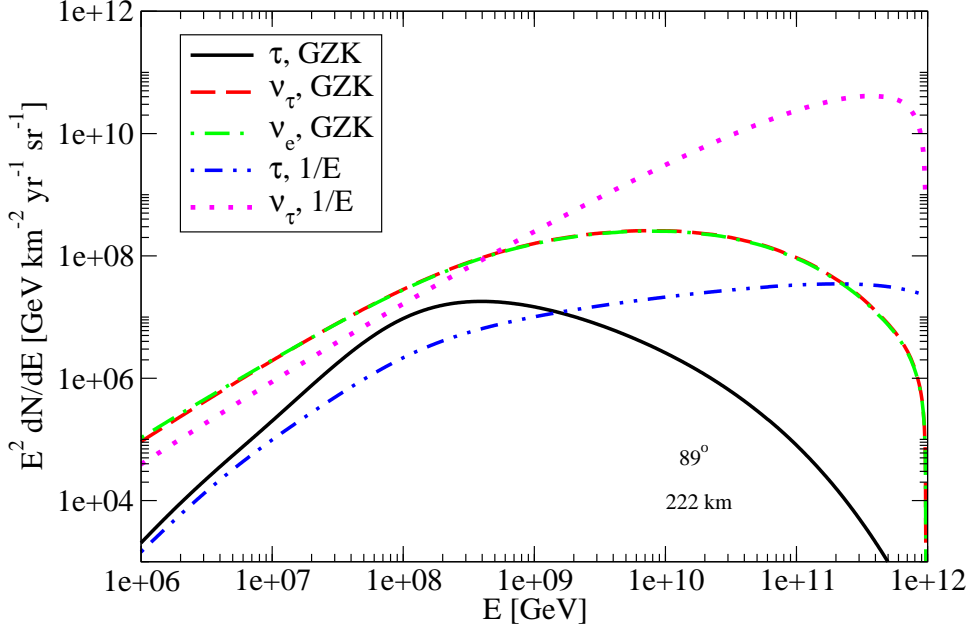


Figure 18: Hadronic shower distributions for detection over 222 km of ice. The ν_μ distribution for GZK neutrinos is the same with that of ν_τ . For the $1/E$ flux all neutrino distributions are almost the same.

80°. We are particularly interested in the contribution from tau neutrinos, produced in oscillations of extragalactic muon neutrinos as they travel large astrophysical distances. After propagation over very long distances, neutrino oscillations change an initial (source) flavor ratio of 1 : 2 : 0 to 1 : 1 : 1 because of the maximal $\nu_\mu \leftrightarrow \nu_\tau$ mixing. For GZK neutrinos, the flavor ratio at Earth deviates from 1:1:1 because the incident fluxes are different. At lower energies and smaller nadir angles, tau neutrino pileups from regeneration via $\nu_\tau \rightarrow \tau \rightarrow \nu_\tau$ [3, 4] enhanced electromagnetic and hadronic signals in kilometer-sized detectors. Our aim here was to see if there are similar effects at high energy.

In our propagation of neutrinos and charged leptons through the Earth, we have focused on kilometer-sized neutrino detectors, such as ICECUBE and RICE and on a detector with much larger effective area which uses Antarctic ice as a converter, ANITA. Our study can easily be generalized to

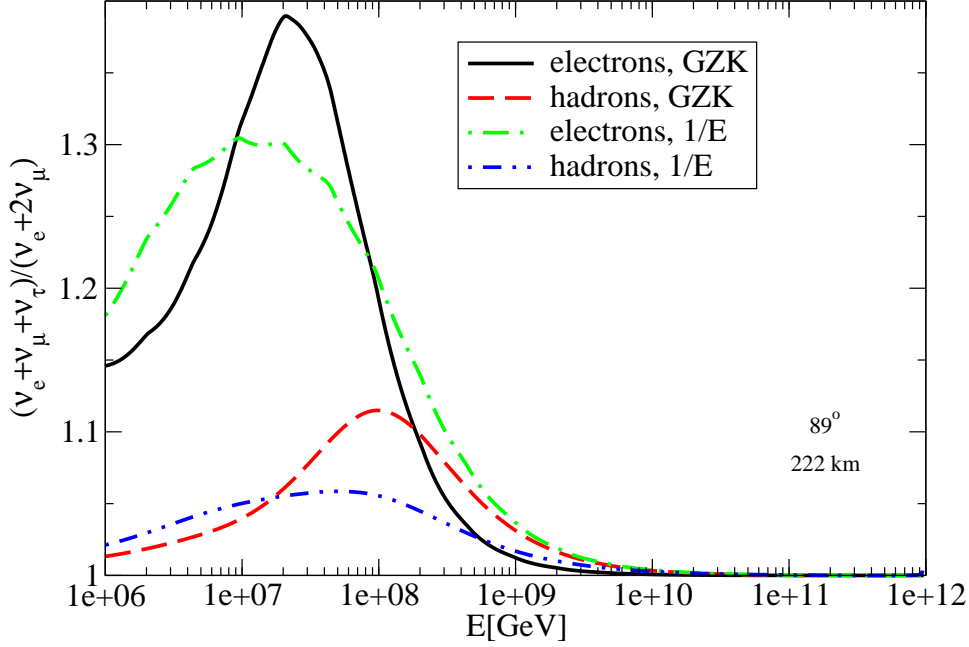


Figure 19: Ratio of electromagnetic and hadronic shower rates in the presence and absence of $\nu_\mu \rightarrow \nu_\tau$ oscillations for GZK and $1/E$ fluxes of neutrinos for detection over 222 km of ice.

other experiments and to propagation in materials other than ice.

We have found that the ν_τ flux above 10^8 GeV resembles the ν_μ flux. The lore that the Earth is transparent to tau neutrinos is not applicable in the high energy regime. Tau neutrino pileups at small angles with respect to the horizon are significantly damped due to tau electromagnetic energy loss above $E_\tau \sim 10^8$ GeV if the column depth is at least as large as the neutrino interaction length.

At lower energies, $E \leq 10^8$ GeV, regeneration of ν_τ becomes important for trajectories where the other flavors of neutrinos are strongly attenuated. The regeneration effect depends strongly on the shape of the initial flux and it is larger for flatter fluxes. The enhancement due to regeneration also depends on the amount of material traversed by neutrinos and leptons, i.e. on nadir angle. For GZK neutrinos, we have found that the enhancement peaks between 10^6 and a few $\times 10^7$ GeV depending on trajectory. For 85° the enhancement is about a factor of two, while for 80° it is a factor of three.

We have translated the neutrino fluxes and tau lepton fluxes into rates

for electromagnetic and hadronic showers at selected angles to see the effect of attenuation, regeneration, and the different energy dependences of the incident fluxes. We have focused on comparing the ν_τ contribution to the ν_e and ν_μ contributions to determine in what range, if any, ν_τ 's enhance shower rates.

The ν_τ flux enhancements depend on the shape of the initial flux. The electromagnetic showers are more sensitive to this shape than hadronic ones. The relative enhancement in hadronic showers is also smaller than for the electromagnetic showers. This is because for the electromagnetic signal the only contribution in the absence of taus is from electron neutrinos, while for hadrons the tau contribution is compared to a much larger signal, from the interactions of all flavors of neutrinos. We have included contribution from secondary neutrinos, which we find to be relatively small for all fluxes.

For kilometer-sized detectors, at for example a nadir angle of 85° , the maximal enhancement due to ν_τ contribution to electromagnetic shower rates for the GZK flux is about 50% at 3×10^7 GeV, while for the $1/E$ flux, it is even larger, about 70%, at slightly lower energy. In the case of hadronic showers for which the events identified by muon tracks have been removed, the ν_τ contribution peaks at about 2×10^7 GeV and it gives an enhancement of about a factor of 1.8 for the GZK flux. These energy ranges are relevant for IceCube, but not for RICE. For energies relevant to RICE, tau neutrinos do not offer any appreciable gain in electromagnetic shower signals compared to $\nu_e \rightarrow e$ CC interactions, and they contribute at essentially the same level as ν_μ to hadronic shower rates through NC interactions.

One of the reasons that tau neutrinos do not contribute large signals to kilometer-sized detectors at very high energies is that high energy tau decay lengths are very large, so the probability of a tau decaying in the detector is low. For detectors like ANITA which can sample long trajectories through the ice one would expect a larger tau neutrino contribution to the signal from tau decay. Despite the long trajectory (222 km with a maximum depth of 1 km for a neutrino incident at 89° nadir angle) the tau contributions to the electromagnetic shower rate is quite small for fluxes expected to contribute in the ANITA signal. For hadronic showers, the suppression of τ decay to hadrons relative to ν_e NC interaction contributions is about the same as for electromagnetic showers compared to $\nu_e \rightarrow e$. The ν_τ contribution to the hadronic shower rate from interactions is the same as the ν_e contribution. In summary, for ANITA, tau neutrinos do not give any additional signal beyond what one would evaluate based on no regeneration from $\nu_\tau \rightarrow \tau \rightarrow \nu_\tau$ due to

tau electromagnetic energy loss at $E \gtrsim 10^8$ GeV.

In addition to the experiments discussed here, there are many studies concerning the possibility for detection of radio Cherenkov emission from showers in materials other than ice. It has been noted [27] that rock salt formations have similar properties to the Antarctic ice and can therefore be used as large scale neutrino detectors. Salt has a higher density ($\rho_{salt} = 2.2$ g/cm³) than ice ($\rho_{ice} = 0.9$ g/cm³), so it is possible to achieve an effective detection volume of several hundred km³ water equivalent in salt. This is somewhat larger than RICE, achieved with a much smaller actual detector size. The threshold for detecting the radio signal from showers in salt is of the order of $\sim 10^7$ GeV, similar to RICE, but lower, such that detection of extra signals from ν_τ enhancements would be more promising.

Also proposed is LOFAR [28], a digital telescope array designed to detect radio Cherenkov emission in air showers. LOFAR has sensitivity in an energy range of $\sim 10^5 - 10^{11}$ GeV, so it can detect showers at much lower energies than other radio Cherenkov experiments. LOFAR will likely be configured to detect horizontal showers from skimming neutrinos as well. With its low energy threshold, LOFAR has an excellent opportunity to observe the shower enhancement at lower energies due to ν_τ regeneration and tau pileup, which is not easily accessible in ANITA.

6 Acknowledgments

This research was supported in part by the National Science Foundation under Grant No. PHY99-07949 and under DOE Contracts DE-FG02-91ER40664, DE-FG02-95ER40906 and DE-FG02-93ER40792. I.M. and I.S. thank KITP Santa Barbara for hospitality. M.H.R. and I.S. thank the Aspen Center for Physics for hospitality while this work was being completed.

References

- [1] Y. Fukuda et al. [Super-Kamiokande Collaboration], Phys. Rev. Lett. **81** (1998), 1562.
- [2] D. V. Ahluwalia, C. A. Ortiz, G. Z. Adunas, hep-ph/0006092; H. Athar, M. Jezabek, O. Yasuda, Phys. Rev. **D 62** (2000), 103007.

- [3] F. Halzen, D. Saltzberg, Phys. Rev. Lett. **81** (1998), 4305; S. Iyer, M. H. Reno, I. Sarcevic, Phys. Rev. **D 61** (2000), 053003; S. Iyer Dutta, M. H. Reno, I. Sarcevic, Phys. Rev. **D 64** (2001), 113015.
- [4] S. Iyer Dutta, M. H. Reno, I. Sarcevic, Phys. Rev. **D 62** (2000), 123001.
- [5] D. Fargion, Astrophys. J. **570** (2002), 909; J. L. Feng, P. Fisher, F. Wilczek, T. M. Yu, Phys. Rev. Lett. **88** (2002), 161102; J. J. Tseng
- [6] T. W. Yeh, H. Athar, M. A. Huang, F. F. Lee, G. L. Lin astro-ph/0305507.
- [7] <http://icecube.wisc.edu> ; Ahrens et al. ICECUBE Collaboration, astro-ph/0305196.
- [8] G. A. Askarian, Soviet Physics, JETP **14** (1962), 441
- [9] I. Kravchenko et al. [RICE Collaboration], astro-ph/0206371, astro-ph/0306408.
- [10] P. Gorham et al. [ANITA Collaboration]
<http://www.ps.uci.edu/~barwick/anitaprop.pdf>.
- [11] G. Barenboim and C. Quigg, Phys. Rev. D **67** (2003) 073024.
- [12] R. Engel, D. Seckel, T. Stanev, Phys. Rev. **D64** (2001), 093010.
- [13] S. Yoshida, H. Dai, C. Jui, P. Sommers, Astrophys. J. **479** (1997), 5471.
- [14] D. Fargion, B. Mele, A. Salis, Astrophys. J. **517** (1999), 725; T. J. Weiler, Astropart. Phys. **11** (1999), 303; S. Yoshida, G. Sigl, S. Lee, Phys. Rev. Lett. **81** (1998), 5505.
- [15] Z. Fodor, S. D. Katz and A. Ringwald, Phys. Rev. Lett. **88** (2002), 171101; Z. Fodor, S. D. Katz and A. Ringwald, JHEP **0206** (2002), 046; O. E. Kalashev, V. A. Kuzmin, D. V. Semikoz and G. Sigl, Phys. Rev. D **65** (2002), 103003.
- [16] K. Mannheim, R. J. Protheroe, J. P. Rachen, Phys. Rev. **D63** (2001), 023003.

- [17] X. Bertou, P. Billoir, O. Deligny, C. Lachaud, A. Letessier-Selvon, *Astropart. Phys.* **17** (2002), 183; S. Bottai, S. Giurgola, *Astropart. Phys.* **18** (2003), 539; K. Giesel, J. H. Jureit, E. Reya, astro-ph/0303252; D. Fargion, M. Khlopov, R. Konoplich, P. G. De Sanctis Lucentini, M. De Santis, B. Mele, astro-ph/0303233; J. F. Beacom, N. F. Bell, D. Hooper, S. Pakvasa, T. J. Weiler, hep-ph/0307025.
- [18] S. Iyer Dutta, I. Mocioiu, M. H. Reno, I. Sarcevic, *Proc. of ICRC 2003*, hep-ph/0307210; T. Montaruli, *Proc. of ICRC 2003*; S. Yoshida, *Proc. of ICRC 2003*.
- [19] R. Gandhi, C. Quigg, M. H. Reno, I. Sarcevic, *Astropart. Phys.* **5** (1996), 81, *Phys. Rev.* **D58** (1998), 093009.
- [20] S. Iyer Dutta, M. H. Reno, I. Sarcevic, D. Seckel, *Phys. Rev.* **D63** (2001) 094020.
- [21] PREM: A. M. Dziewonsky and D. L. Anderson, *Phys. Earth. Planet. Inter* **25** (1981) 297; REM (Reference Earth Model): S.V. Panasyuk, <http://cfauvcs5.harvard.edu/lana/rem/index.htm>; <http://mahi.ucsd.edu/Gabi/rem.html>; P. M. Shearer, *Introduction to Seismology* (Cambridge, 1999); B. Romanowicz, *Geophys. Res. Lett.*, **28** (2001) 1107.
- [22] J. Pumplin, D. R. Stump, J. Huston, H. L. Lai, P. Nadolsky, and W. K. Tung [CTEQ Collaboration], *JHEP* 0207 (2002) 012.
- [23] J. Beacom, P. Crotty and E. W. Kolb, *Phys. Rev.* **D66** (2002), 021302.
- [24] S. Iyer Dutta, M. H. Reno and I. Sarcevic, *Phys. Rev.* **D66** (2002), 077302.
- [25] J. Learned, S. Pakvasa, *Astropart. Phys.* **3** (1995), 267.
- [26] AMANDA Collaboration, astro-ph/0306536, astro-ph/0306209 .
- [27] P. Gorham et al. *Nucl. Instrum. Meth.* **A490** (2002), 476
- [28] H. Falcke, P. Gorham, *Astropart. Phys.* **19** (2003), 477.